ACS Editors' Choice

JACS
JOURNAL OF THE AMERICAN CHEMICAL SOCIETY

Communication

pubs.acs.org/JACS

Terms of Use

Hydrogen Production from Ammonia Using Sodium Amide

William I. F. David,*[,†,‡] Joshua W. Makepeace,[†,‡] Samantha K. Callear,[†] Hazel M. A. Hunter,[†] James D. Taylor,[†] Thomas J. Wood,[†] and Martin O. Jones[†]

[†]ISIS Facility, Rutherford Appleton Laboratory, Harwell Oxford, Didcot OX11 0QX, U.K.

[‡]Inorganic Chemistry Laboratory, University of Oxford, Oxford OX1 3QR, U.K.

Supporting Information

ABSTRACT: This paper presents a new type of process for the cracking of ammonia (NH_3) that is an alternative to the use of rare or transition metal catalysts. Effecting the decomposition of NH_3 using the concurrent stoichiometric decomposition and regeneration of sodium amide ($NaNH_2$) via sodium metal (Na), this represents a significant departure in reaction mechanism compared with traditional surface catalysts. In variable-temperature NH_3 decomposition experiments, using a simple flow reactor, the Na/$NaNH_2$ system shows superior performance to supported nickel and ruthenium catalysts, reaching 99.2% decomposition efficiency with 0.5 g of $NaNH_2$ in a 60 sccm NH_3 flow at 530 °C. As an abundant and inexpensive material, the development of $NaNH_2$-based NH_3 cracking systems may promote the utilization of NH_3 for sustainable energy storage purposes.

The Haber–Bosch process for the industrial synthesis of ammonia has, over the past century, led to a global revolution in agriculture to the extent that almost half the crops grown across the world today depend on ammonia-based fertilizers.[1] The reverse reaction may have a similarly transformative potential, where the decomposition of ammonia into nitrogen and hydrogen enables the provision of hydrogen for a low-carbon energy economy.[2] Indeed, high-density, affordable, and efficient hydrogen storage is one of the key steps in the realization of a hydrogen-based energy sector.[3]

Hydrogen (H_2) is an attractive chemical fuel, with very high gravimetric energy content (120 MJ/kg) and an emissions profile free from carbon dioxide. Despite these advantages, its use has been hindered by the lack of an effective and efficient method for its storage. Current high-pressure (~700 bar) storage is expensive and energy-intensive, and imposes practical restrictions on tank dimensions. In response to this challenge, there has been a significant research effort over the past 15 years that has focused on new chemical hydrogen storage materials, particularly solid-state materials which offer impressive volumetric and gravimetric hydrogen densities.[4] Arguably, this focus may have diminished the consideration of reversibility, cost, and practicality of use of these materials. To date, very few candidates show potential beyond that of the seminal work on titanium-doped sodium alanate.[5]

Ammonia (NH_3) has a high gravimetric (17.8 wt% H_2) and volumetric (121 kg H_2 m^{-3} in the liquid form) H_2 density and is produced on an industrial scale. Furthermore, it has an existing extensive distribution network and is easily stored by liquefaction at moderate pressure (ca. 10 bar at room temperature). While both perceived and real safety risks due to the toxicity of NH_3 have detracted from its appeal, its adoption as a vector for H_2 has not yet been realized largely because of the absence of an efficient, low-cost method for cracking NH_3 to H_2 and N_2.[6]

Although extensively used as a reagent in a variety of synthesis processes,[7] sodium amide ($NaNH_2$) has attracted only passing interest from the hydrogen storage community.[8] Its low melting point and high chemical reactivity make conventional analysis methods challenging. Moreover, its modest H_2 capacity and high decomposition enthalpy (ΔH = 123.8 kJ mol^{-1}) suggest, on initial consideration, that $NaNH_2$ is an unattractive H_2 storage candidate. However, as first observed by Titherley in 1894,[9] and confirmed in 1937 by Sakurazawa and Hara,[10] $NaNH_2$ decomposes to its constituent elements (eq 1). The formation of two gases results in an unusually large entropy change, ΔS = 200.9 J K^{-1} mol^{-1}, that leads to a modest theoretical decomposition temperature of 343 °C.[11] Bulk production of $NaNH_2$ is by reaction of sodium metal (Na) with gaseous (or liquid) NH_3, according to eq 2.[12]

$$NaNH_{2(s)} \rightarrow Na_{(s)} + {}^1/_2\, N_{2(g)} + H_{2(g)} \quad (1)$$

$$Na_{(s)} + NH_{3(g)} \rightarrow NaNH_{2(s)} + {}^1/_2\, H_{2(g)} \quad (2)$$

Run concurrently, these two reactions should effect the chemical decomposition of NH_3 by cycling between sodium amide and sodium metal (eq 3).

$$2NH_{3(g)} \xrightarrow{Na+NaNH_2} N_{2(g)} + 3H_{2(g)} \quad (3)$$

In 1894, Titherley noted this property in passing, stating that "an interesting result is obtained on heating sodamide to dull redness ... through which a current of ammonia is passing; the latter is continuously decomposed into its elements". Remarkably, this reaction has not been further studied nor its use and application examined since.

Here we present the detailed conditions and discuss the mechanism of NH_3 decomposition by $NaNH_2$. Using a simple flow reactor, we demonstrate high NH_3 decomposition efficiencies over extended periods at moderate temperatures.

Existing catalysts for low-temperature NH_3 cracking are predominantly based on transition metals. Ruthenium shows the highest catalytic activity which is enhanced when the metal is

Received: May 7, 2014
Published: June 22, 2014

impregnated into complex support microstructures with promoter species.[13−16] Our results indicate that the performance of as-found $NaNH_2$ for continuous stoichiometric NH_3 decomposition is as effective as a supported ruthenium catalyst. The material costs, however, are very significantly less. We believe this combination of high efficiency and low cost of the $Na/NaNH_2$ system indicates the potential of this new class of NH_3 decomposition catalyst, and invites reconsideration of the potential of NH_3 decomposition as a viable delivery method of H_2, for applications ranging from small-scale distributed power to massive grid-balancing and on-board use for transportation.

The NH_3 decomposition reactions were performed in simple cylindrical flow reactors (316 stainless steel) of internal volume 46.9 or 21.3 cm^3, Figure 1a (see also Supporting Information).

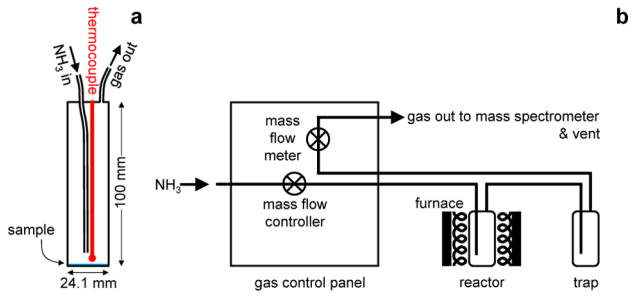

Figure 1. Reactor and experimental setup: (a) A typical 46.9 cm^3 reactor showing NH_3 inlet, gas outlet, and thermocouple temperature probe positions, with 0.5 g $NaNH_2$, drawn to scale. (b) Experimental setup, where the inlet NH_3 gas flow is controlled prior to the reactor, and the outlet gas flow is monitored by a mass flow meter and analyzed by a mass spectrometer.

NH_3 gas (99.98%) was supplied to the reactor via a custom-designed gas control panel (Figure 1b) where the exhaust gas stream was quantitatively analyzed by a Hiden Analytical HPR-20 mass spectrometer (Quantitative Gas Analysis, QGA) calibrated with a certified gas mixture of composition 2% NH_3, 2% H_2, 2% N_2, and 94% Ar (balance). A typical experiment comprised loading 0.5 g catalyst powder ($NaNH_2$, Ni-SiO_2-Al_2O_3, or Ru-Al_2O_3) into the reactor under argon with experiments performed at atmospheric pressure where the system was operated either at a constant flow (60 sccm NH_3) while varying the reaction temperature or at constant temperature while varying the NH_3 inlet flow. Gas flows were recorded in standard cubic centimeters per minute (sccm). Neutron diffraction data were collected on the POLARIS instrument[17] at ISIS, for 4 h at room temperature, from approximately 0.2 g post-reaction powder samples contained within quartz capillaries. Rietveld refinement was performed using TOPAS Academic.[18]

If the decomposition of NH_3 is stoichiometric, then the reaction only involves interconversion between $NaNH_2$ and Na metal as described in eqs 1 and 2. To confirm this hypothesis, reactions were performed under flowing NH_3 (20−60 sccm) using both $NaNH_2$ and Na metal as initial reactants (Figure 2, panels a and b, respectively), and the outgas was examined using QGA. On heating, the $NaNH_2$ sample (Figure 2a) shows a small peak in the N_2 signal at 155 °C, which is consistent with the release of occluded or adsorbed N_2 remnant from the synthesis of $NaNH_2$. For the Na sample (Figure 2b), a peak in the H_2 signal at 330 °C is associated with the formation of $NaNH_2$ from Na as detailed in eq 2. The QGA data show, as expected, that significant NH_3 decomposition is observed for both samples above 360 °C and that this increases with temperature. Over the duration of

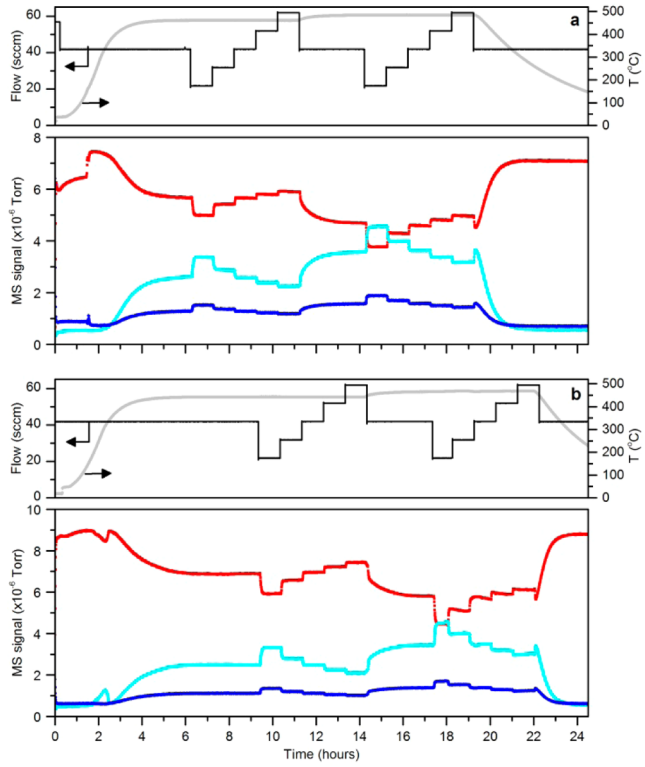

Figure 2. Ammonia decomposition reaction mass spectrometry traces for NH_3 (red, $m/z = 17$), H_2 (cyan, $m/z = 2$), and N_2 (blue, $m/z = 28$) for the reaction of (a) 0.25 g of $NaNH_2$ and (b) 0.15 g of Na. The temperature (light gray) and NH_3 flow rate (dark gray) during the experiment at atmospheric pressure are indicated in the top panels for each reaction.

each of these experiments, $NaNH_2$ decomposes more than 100 mol equiv of NH_3. This suggests that the H_2 and N_2 produced in these experiments result from a catalytic cycle rather than any other process.

At temperatures between 300 and 600 °C, Na and $NaNH_2$ exist in equilibrium, with Na favored at higher temperatures as $NaNH_2$ becomes less stable. Neutron powder diffraction analysis of the samples post-reaction (see Supporting Information, Figures S2 and S3) identified $NaNH_2$ as the major crystalline component in both samples, with a small amount of Na (~12 wt%) detected in the sample originally present as $NaNH_2$. Given that there is no obvious H_2 peak or increase in the hydrogen-to-nitrogen ratio upon cooling, such as would result from the conversion of Na back to $NaNH_2$ (see eq 2), these data indicate that $NaNH_2$ is the major species at the temperatures of the experiments shown in Figure 2.

The use of neutron powder diffraction also enables the stoichiometry of each amide sample to be evaluated, as non-stoichiometric species have been shown to be an integral part of NH_3-mediated processes in the lithium amide−lithium hydride hydrogen storage composite.[19,20] Rietveld analysis of each neutron diffraction pattern returned hydrogen site occupancies of 0.99(4) for the $NaNH_2$ sample and 1.00(3) for the Na sample, indicating that the amide is indeed stoichiometric. We conclude that our results are consistent with the reaction mechanism outlined in eqs 1−3 for the action of $Na/NaNH_2$ on NH_3.

The NH_3 decomposition efficiencies of a selection of relevant catalyst powders, tested at a constant 60 sccm flow of NH_3 across various temperatures, are shown in Figure 3. We have used these

dx.doi.org/10.1021/ja5042836 | J. Am. Chem. Soc. 2014, 136, 13082−13085

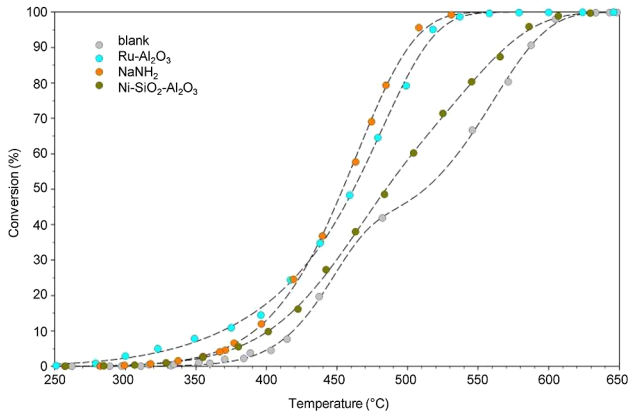

Figure 3. Comparison of NH_3 conversion as a function of reaction temperature (between 250 and 650 °C) for the blank 46.9 cm^3 reactor and 0.5 g of $NaNH_2$, silica/alumina-supported nickel, and alumina-supported ruthenium, at an NH_3 flow rate of 60 sccm. The data were fitted to a sigmoidal distribution (see Supporting Information).

data to compare the performance of $NaNH_2$ to equivalent masses of alumina-supported ruthenium and silica/alumina-supported nickel catalysts. We observe 90% NH_3 decomposition efficiency at 500 °C using $NaNH_2$, relative to 82% and 58% conversion at this temperature using the ruthenium and nickel catalysts, respectively. Under the conditions of these experiments, the supported nickel catalyst offers only marginal improvement over the performance of the blank steel reactor. This is consistent with the use of nickel generally being confined to high-temperature (~900 °C) production of reducing atmospheres for metal heat treatment. Ruthenium is generally accepted to be the most active catalyst for the decomposition of NH_3. The variable-temperature decomposition efficiency of $NaNH_2$ is similar to that of the supported ruthenium catalyst in Figure 3, with superior performance at high conversion values, while the ruthenium catalyst appears to be more active at lower temperatures.

Recent catalyst studies have demonstrated that the ruthenium catalysts benefit from the development of more sophisticated supports,[21] along with additive materials[14] and more optimized reactor design.[15] Indeed, the 2004 study by Yin et al.[13] of potassium hydroxide-modified ruthenium supported on a magnesia−carbon nanotube composite shows almost 100% NH_3 decomposition efficiency at 500 °C with 0.1 g of sample and an NH_3 flow rate of 100 sccm. Nickel−ruthenium composite catalyst systems, which have been scaled up to kW scale stationary cracking units, show a decomposition efficiency of 99.99% at 500 °C and 485 sccm of NH_3 using 20 g of catalyst in a packed tube reactor.[22] These results are evidently superior to those obtained for ruthenium and $NaNH_2$ in this study. However, the comparison in Figure 3 highlights the significant potential and impressive performance of $NaNH_2$, with the unmodified powder achieving >90% conversion at a lower temperature than supported ruthenium. Given the significant scope for optimization of the operating parameters and variation in the form and method of presenting of $NaNH_2$, we anticipate that $NaNH_2$-based NH_3 decomposition will perform as well as the best ruthenium-based catalysts at a very significantly reduced materials cost.

Two of the most promising routes for enhancing NH_3 conversion efficiencies lie in improving the containment and increasing the active reaction surface area of Na/$NaNH_2$. At the temperatures of operation, both $NaNH_2$ and Na are present as an aerosol within the reactor and as a covering of the reactor base and walls. With current reactor volumes and amounts of $NaNH_2$, the aerosol density will be low (~2% of the liquid density), while any covering of the reactor base and walls will be thin. Furthermore, material loss from the reactor is occasionally observed in our experiments over a period of several hours. To improve both material containment and reaction surface area, a 1.6 mm thick nickel-foam baffle was placed 5 mm above the bottom of the NH_3 inlet tube (Figure S1). The results of these experiments, undertaken at 475 °C and at variable flow rate in a 46.9 cm^3 reactor, are shown in Figure 4a. Four sets of data are

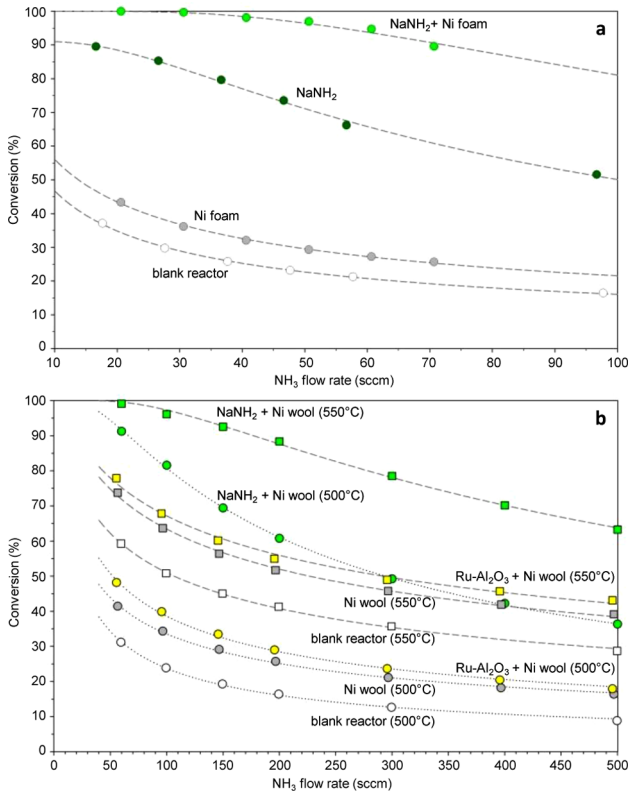

Figure 4. Impact of containment methods. (a) Conversions obtained at 20−100 sccm flow within a 46.9 cm^3 reactor for 0.5 g of $NaNH_2$ at ~475 °C in the presence of a Ni foam barrier (1.6 mm height). Data for a blank reactor, Ni foam (only), and 0.5 g of $NaNH_2$ (only) are shown for reference. (b) Conversions obtained at higher NH_3 flows (50−500 sccm), within a 21.3 cm^3 reactor, for 0.5 g of $NaNH_2$ (green symbols) at ~500 °C (solid circles) and ~550 °C (solid squares) in the presence of 2 g of nickel wool. The corresponding (i) alumina-supported ruthenium with 2 g of nickel wool (yellow symbols), (ii) 2 g of nickel wool only (gray symbols), and (iii) blank reactor data (open symbols) are shown for reference.

shown. The blank reactor alone produces an NH_3 conversion efficiency of 30−40% while the inclusion of the baffle increases this efficiency by another 10%. $NaNH_2$ (0.5 g) within the reactor has an efficiency of 88.5% at low flow rates (20 sccm); the addition of the baffle results in a measured efficiency of 99.98% and 96.5% at 20 and 50 sccm NH_3 flow rates, respectively. These data indicate that the nickel baffle plays a significant role in enhancing the surface area/containment of the Na/$NaNH_2$. This first step in the improvement of NH_3 conversion efficiency suggests that future reactor designs will lead to greatly improved performance. Higher NH_3 flow rates (up to 500 sccm) have also been explored. Conversion efficiencies for 0.5 g of $NaNH_2$ with 2.0 g of nickel wool at three temperatures are shown in Figure 4b.

dx.doi.org/10.1021/ja5042836 | J. Am. Chem. Soc. 2014, 136, 13082−13085

The highest measured H_2 production rate (at 550 °C) is 475 sccm, corresponding to 63.3% conversion efficiency of a 500 sccm NH_3 flow. The conversion rates for the Ni wool alone were only marginally better than the rates observed for the blank reactor, indicating that the wool plays an effective containment role but has little catalytic effect at these temperatures.

Light metal amides clearly show significant potential as a new class of catalyst for the effective, efficient, and inexpensive decomposition of NH_3 into H_2 and N_2. Of course, their potential to catalyze the formation of NH_3 is also worthy of investigation, though the catalytic activity may be diminished under the different pressure regime required for NH_3 synthesis. For the application of NH_3 decomposition, low-temperature fuel cells—either alkaline fuel cells or proton exchange membrane-based—are well placed to utilize the H_2 produced. Given that a 1 kW fuel cell requires a H_2 supply of ~13.5 L/min,[6] linear scale-up of the highest production rate from Figure 4b to this power output would require a reactor volume of 0.62 L, using 14.5 g of $NaNH_2$. However, the direct combustion of NH_3 is, perhaps, the most attractive short-term option. NH_3 alone is difficult to ignite, but a 2.5 wt% hydrogen-in-ammonia mixture is sufficient to enable NH_3 combustion.[23] Indeed, a recent high-performance car achieved a range of 180 km with a 30 L NH_3 tank.[24] Using the current best conversion rates obtained in our experiments, this mix could be provided, at sufficient flow rates, using a total reactor volume of 3.2 L, containing 75 g of $NaNH_2$ (see Supporting Information for full calculation).

These calculations indicate that ammonia-based transportation is achievable. While advances in the containment and turnover frequency of the amide are necessary steps toward this goal, we anticipate that significant improvements in these areas will be realized through the optimization of the reactor design and materials properties of $NaNH_2$.

In summary, we have shown that sodium amide is an effective ammonia decomposition catalyst that involves the stoichiometric decomposition and formation of $NaNH_2$ from Na metal. This approach is a departure from traditional transition metal catalysis and opens up a new class of amide-based materials for the delivery of hydrogen from ammonia for use in sustainable energy applications.

■ ASSOCIATED CONTENT

Ⓢ Supporting Information

Extended methods, raw data, data fitting procedures, and scale-up calculations. This material is available free of charge via the Internet at http://pubs.acs.org.

■ AUTHOR INFORMATION

Corresponding Author

bill.david@stfc.ac.uk

Notes

The authors declare no competing financial interest.

■ ACKNOWLEDGMENTS

The authors thank Mark Kibble, Leigh Perrott, Richard Haynes, Christopher Goodway, and Jon Bones for technical support, Ronald Smith for assistance collecting the neutron diffraction data, Alistair Overy for help with data collection, and Kate Ronayne, Steven Wakefield, Tim Bestwick, and Andrew Taylor for project management and helpful discussions. This work was financially supported by an STFC Innovations Proof of Concept Award (Phase 3 POCF1213-14). J.W.M. thanks the Rhodes Trust for funding.

■ REFERENCES

(1) Erisman, J. W.; Sutton, M. A.; Galloway, J.; Klimont, Z.; Winiwarter, W. *Nat. Geosci.* **2008**, *1*, 636−639.

(2) (a) Green, L., Jr. *Int. J. Hydrogen Energy* **1982**, *7*, 355−359. (b) Avery, W. *Int. J. Hydrogen Energy* **1988**, *13*, 761−773. (c) Lan, R.; Irvine, J. T. S.; Tao, S. *Int. J. Hydrogen Energy* **2012**, *37*, 1482−1494. (d) Klerke, A.; Christensen, C. H.; Nørskov, J. K.; Vegge, T. *J. Mater. Chem.* **2008**, *18*, 2304−2310. (e) Christensen, C. H.; Johannessen, T.; Sørensen, R. Z.; Nørskov, J. K. *Catal. Today* **2006**, *111*, 140−144.

(3) Schlapbach, L.; Züttel, A. *Nature* **2001**, *414*, 353−358.

(4) (a) Li, H.-W.; Yan, Y.; Orimo, S.; Züttel, A.; Jensen, C. M. *Energies* **2011**, *4*, 185−214. (b) Huang, Z.; Autrey, T. *Energy Environ. Sci.* **2012**, *5*, 9257−9268.

(5) Schwickardi, M.; Bogdanovic, B. *J. Alloys Compd.* **1997**, *254*, 1−9.

(6) Thomas, G.; Parks, G. *Potential Roles of Ammonia in a Hydrogen Economy*; U.S. Department of Energy: Washington, DC, 2006; pp 1−23.

(7) Caubere, P. *Acc. Chem. Res.* **1974**, *7*, 301−308.

(8) (a) Chater, P. A.; Anderson, P. A.; Prendergast, J. W.; Walton, A.; Mann, V. S. J.; Book, D.; David, W. I. F.; Johnson, S. R.; Edwards, P. P. *J. Alloys Compd.* **2007**, *446−447*, 350−354. (b) Liu, A.; Song, Y. *J. Phys. Chem. B* **2011**, *115*, 7−13. (c) Xiong, Z.; Hu, J.; Wu, G.; Chen, P. *J. Alloys Compd.* **2005**, *395*, 209−212.

(9) Titherley, A. W. *J. Chem. Soc.* **1894**, *65*, 504−522.

(10) Sakurazawa, K.; Hara, R. *J. Soc. Chem. Ind. (Japan) Suppl.* **1937**, *40*, 10B.

(11) David, W. I. F. *Faraday Discuss.* **2011**, *151*, 399−414.

(12) Juza, R. *Angew. Chem., Int. Ed.* **1964**, *3*, 471−481.

(13) Yin, S. F.; Xu, B. Q.; Wang, S. J.; Ng, C. F.; Au, C. T. *Catal. Lett.* **2004**, *96*, 113−116.

(14) Raróg-Pilecka, W.; Szmigiel, D.; Kowalczyk, Z.; Jodzis, S.; Zielinski, J. *J. Catal.* **2003**, *218*, 465−469.

(15) Sørensen, R. Z.; Nielsen, L. J. E.; Jensen, S.; Hansen, O.; Johannessen, T.; Quaaded, U.; Christensen, C. H. *Catal. Commun.* **2005**, *6*, 229−232.

(16) Klerke, A.; Klitgaard, S. K.; Fehrmann, R. *Catal. Lett.* **2009**, *130*, 541−546.

(17) Hull, S.; Smith, R. I.; David, W. I. F.; Hannon, A. C.; Mayers, J.; Cywinski, R. *Physica B* **1992**, *180−181*, 1000−1002.

(18) Coelho, A. *TOPAS-Academic*, V4.1; Coelho Software: Brisbane, Australia, 2007; http://www.topas-academic.net/.

(19) David, W. I. F.; Jones, M. O.; Gregory, D. H.; Jewell, C. M.; Johnson, S. R.; Walton, A.; Edwards, P. P. *J. Am. Chem. Soc.* **2007**, *129*, 1594−1601.

(20) Makepeace, J. W.; Jones, M. O.; Callear, S. K.; Edwards, P. P.; David, W. I. F. *Phys. Chem. Chem. Phys.* **2014**, *16*, 4061−4070.

(21) Schüth, F.; Palkovits, R.; Schlögl, R.; Su, D. S. *Energy Environ. Sci.* **2012**, *5*, 6278−6289.

(22) Hacker, V.; Kordesch, K. In *Handbook of Fuel Cells—Fundamentals, Technology and Applications*; Vielstich, W., Lamm, A., Gasteiger, H. A., Eds.; John Wiley & Sons Ltd.: Chichester, 2003; Vol. 3, Part 2, Chap. 10, pp 121−127.

(23) Mørch, C. S.; Bjerre, A.; Gøttrup, M. P.; Sorenson, S. C.; Schramm, J. *Fuel* **2011**, *90*, 854−864.

(24) Toyota GT86-R Marangoni Eco Explorer: sport and technology in the new 2013 show car, fitted with Marangoni "M-Power EvoRed" tyres. Feb 28, 2013; http://www.marangonipress.com/SinglePR.aspx?prid=545 (accessed Jun 6, 2014).